Journal of Power Sources 188 (2009) 177–183

Contents lists available at ScienceDirect

Journal of Power Sources

journal homepage: www.elsevier.com/locate/jpowsour

Modeling of cracking of the glass-based seals for solid oxide fuel cell

Tao Zhang[a,b], Qingshan Zhu[a,*], Zhaohui Xie[a]

[a] State Key Laboratory of Multiphase Complex System, Institute of Process Engineering, Chinese Academy of Sciences, Beijing 100190, People's Republic of China
[b] Graduate University of Chinese Academy of Sciences, Beijing 100049, People's Republic of China

ARTICLE INFO

Article history:
Received 13 October 2008
Received in revised form
16 November 2008
Accepted 17 November 2008
Available online 24 November 2008

Keywords:
SOFC
Seal
Cracking diagram
Seal thickness
CTE mismatch

ABSTRACT

For planar SOFCs the seal is a critical component, potential fracture in the seal needs to be investigated in order to enhance the reliability of the seal. A model based on the classical beam bending theory and the fracture theory of ceramic materials has been developed for predicting the crack extension in the seal. The model reveals that the resistance of the seal to cracking on cooling is mainly affected by two factors: the seal thickness and the CTE mismatch. Furthermore, a cracking diagram is established to reveal the effects of the seal thickness and CTE mismatch on the crack extension behavior. It shows that the 'no cracking' area increases with decreasing seal thickness, and larger CTE mismatch requires a thinner seal to avoid cracking. The model and the cracking diagram are experimentally validated through monitoring the leakage rate of a glass-sealed chamber, and the crack extension deduced from the measured leakage rate shows good agreement with those predicted by the model. The proposed model can serve as a useful tool in sealing design of SOFC.

1. Introduction

Solid oxide fuel cells (SOFCs) are promising energy conversion systems with high conversion efficiency. While providing high power density, the planar SOFC must overcome a significant challenge, that is the need for gastight, high temperature seals to prevent fuel leakage [1]. The majority of the SOFC seal development has been focusing on bonded, rigid seals, primarily glasses and glass–ceramics. Seals need to withstand many thermal cycles during routine operation. During cooling down from operation temperatures, residual thermal stresses will build up in the seals, primarily due to the thermal expansion mismatch between the sealing material and adjacent components. However, glass-based seals are susceptible to fracture due to the brittle nature of glasses and glass–ceramics. Consequently, fracture has been reported to be one of the main failure modes of the glass-based seals [2–6]. It is therefore of significant importance to reduce fracture probability of the glass-based seals in order to enhance the reliability of SOFCs.

In the past decades, much effort has been given to develop glass-based seals of better performance in term of match of the coefficient of thermal expansion (CTE) between the seal and the adjacent components [7–11]. However, residual thermal stress will always exist in the glass-based seal matrix, even if there is a good match of CTE between the seals and adjacent cell components. Therefore, the reliability of the seals needs to be enhanced by other ways, besides optimizing the CTE of the glass-based seals. In fact, optimization of the sealing structure has a significant effect on a reliable sealing of SOFC, which is just the focus of this work.

In practice, there exist two typical failure phenomena: the interfacial debonding of adhesive joints [12] and the cracking of the seal layer [2,3]. The failure mode of the sealing depends on the combination of the seal material and the steel. It is because that the interface, especially the glass/metal interface, may be weak (the interfacial fracture energy is lower than the fracture energy of the seal) [12], but it may be also excellent (the interfacial fracture energy is higher than the fracture energy of the seal) [2,7]. The first case has been addressed recently by Muller et al. [12], where finite element modeling was employed to analyze the residual stress distribution in a typical seal and the crack propagation along the interface. They found that a crack would grow if and only if both the released energy and the local stresses exceed critical values, and the resistance of the seal to debonding would increase with increasing width and decreasing thickness of the seal. But the second case has not yet been well investigated, and the residual stress field and the failure mechanism of the seals have not yet been well clarified. This paper is therefore focused on cracking of the seal.

In the present paper, a model based on the classical beam bending theory and the fracture theory of ceramic materials has been developed for predicting cracking of the SOFC seals. A model reported earlier in Ref. [13], was developed to calculate the residual thermal stress within each layer for a multilayer system cooling

* Corresponding author at: State Key Laboratory of Multiphase Complex System, Institute of Process Engineering, Chinese Academy of Sciences, Zhong Guan Cun, Haidian District, P.O. Box 353, Beijing 100190, People's Republic of China.
Tel.: +86 10 62536108; fax: +86 10 62536108.
E-mail address: qszhu@home.ipe.ac.cn (Q. Zhu).

0378-7753/$ – see front matter.
doi:10.1016/j.jpowsour.2008.11.053

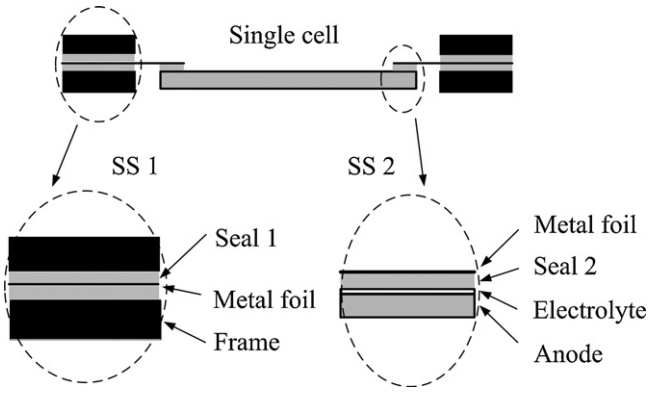

Fig. 1. A typical cell cross section and two types of sealing sections.

down from a stress free temperature due to the thermal expansion difference of different layers. However, the model cannot be used to analyze the cracking of the glass-based seals since the bodies of the seals are usually under biaxial compressive stresses, which will not induce cracking. Analyses revealed that cracking of glass-based seals is mainly caused by the tensile stress at the free surfaces (the edges) of the seals and the tensile stress is related to the compressive stress in the seal body. So, the previous model was further developed to calculate the tensile stress at the free surfaces. Crack extension behavior was then analyzed through applying strain energy release rate criterion. The effects of various material properties and sealing structure on the cracking of the seal have been subsequently investigated based on the model. The model has been validated using experimental data obtained on a sandwich sealing structure consisting of interconnect–seal–interconnect multiple layers.

2. Theoretical analysis

Two typical cross sections of seals in an anode-supported SOFC cell are shown in Fig. 1. From the sealing sections, it can be seen that the components are assembled layer by layer, forming a multilayer system. Layered materials subjected to residual and applied stresses are susceptible to cracking. If the net stress in the seal layer is tensile and sufficiently high, it will drive preexisting flaws to extend into the seal matrix.

The principal stresses within the multilayer systems has been investigated previously by Zhang et al. [13] by the force balance and bending moment balance method, so only a brief description is made here.

A cross section of a multilayer system is shown schematically in Fig. 2, where the thickness of ith layer is t_i. The subscript, i, denotes the layer number ranging from 1 to n, with 1 representing the layer at the bottom. The coordinate system is defined such that the free surface of the 1st layer is located at $z = 0$, and the interface between layers i and $i+1$ is located at $z = h_i$. With these definitions, the relation between h_i and t_i is described by

$$h_i = \sum_{j=1}^{i} t_j \quad (1 \le i \le n, \quad 1 \le j \le i) \tag{1}$$

The residual thermal stresses, σ_i, within the body, when the multilayer system is cooled from a stress free temperature, T_0, to T, are given by

$$\sigma_i = E_i^*[\varepsilon_i + K(z - \delta)] \tag{2}$$

Here

$$\varepsilon_i = \frac{\sum_{j=1}^{n} E_j^* t_j (\alpha_i - \alpha_j)(T_0 - T)}{\sum_{j=1}^{n} E_j^* t_j}$$

$$\delta = \frac{\sum_{i=1}^{n} E_i^* t_i (2h_i - t_i)}{2\sum_{i=1}^{n} E_i^* t_i}$$

$$K = \frac{-3\sum_{i=1}^{n} E_i^* \varepsilon_i [2h_i t_i - t_i^2 - 2\delta t_i]}{2\sum_{i=1}^{n} E_i^* [(h_i - \delta)^3 - (h_i - t_i - \delta)^3]}$$

$$E^* = \frac{E}{1 - \nu}$$

where the subscripts, i and j, denote the ith and jth layers; E, ν and α are the elastic modulus, the Poisson's ratio and the coefficient of thermal expansion, respectively; the parameter δ is the distance from the bending axis to the free surface of the 1st layer ($z = 0$) and K is the curvature [13].

Actually, the CTE of the common seal used in SOFC stacks is lower than that of the interconnect or the anode, the bodies of the seal are therefore under biaxial compressive stresses, σ_s, which will not induce cracking. However, the stresses at the free surfaces of the seal are different from those within the matrix, and tensile stresses will be present. Fig. 3 illustrates the stress distribution in a layer, which is under biaxial compressive stresses in the plane, in a multilayer system; at its edge, there is a tensile stress normal to the interface. The stress distribution in the seal in SS 1 or SS 2 geometry is similar to it. These surface tensile stresses, perpendicular to the layer plane, can cause extension of the preexisting cracks. This

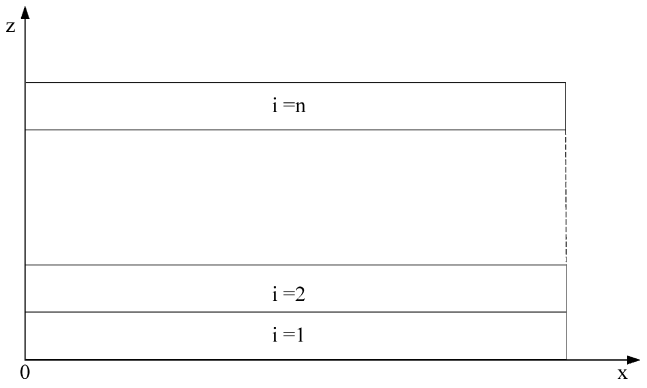

Fig. 2. Cross section of a multilayer system.

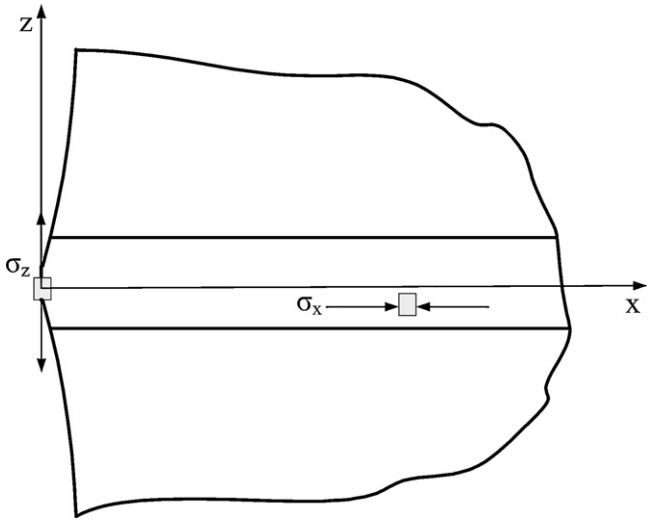

Fig. 3. Schematic of the stress distribution in a layer under biaxial compressive stresses in the plane in a multilayer system; at its edge, there is a tensile stress normal to the interface.

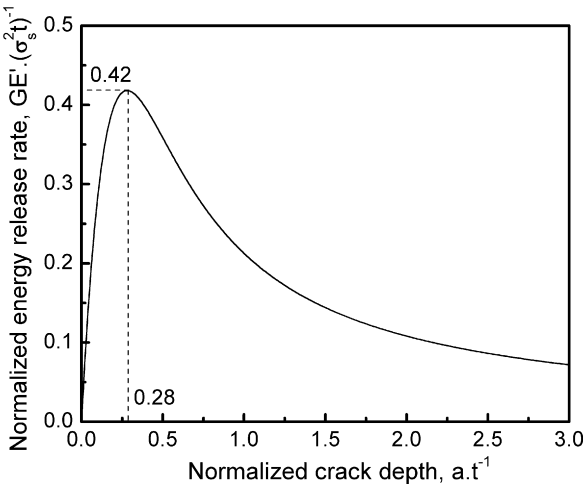

Fig. 4. Normalized energy release rate G varies with normalized crack depth $a{\cdot}t^{-1}$ [14].

type of crack propagation has been analyzed by Ho et al. [14]. As illustrated in Fig. 3, the thin seal layer strives to contract less than the two adjacent layers, bending its surface and thereby inducing the tensile stress, σ_z. In this coordinate system, it is defined such that the centerline of the seal layer coincides with the x-axis. On the surface ($x=0$), σ_z is a step-function, equal to σ_s in the seal layer, $\sigma_s/2$ at the interface, and zero in the next layers. Along the centerline, the tensile stress is given by [14]:

$$\sigma_{z|z=0} = \frac{2}{\pi}\left[\theta - \frac{1}{2}\sin 2\theta\right]\sigma_s \tag{3}$$

where $\tan\theta = t/2x$.

Interacting with the preexisting flaws, the tensile stress, σ_z, may induce crack extension that may cause fracture of the seal. The crack extension is controlled by the energy release rate, where the initiated cracks will propagate into the layer when the strain energy release rate, G, averaged over the virtual crack, is greater than the critical strain energy release rate (fracture energy) of the sealing material.

The strain energy release rate for the crack extension into the layer is given by [14,15]

$$\frac{GE'}{\sigma_s^2 t} = \pi\frac{a}{t}s^2\{1.122 - (1-s)[0.296 + 0.25s^{3/4}(0.75-s)]\}^2 \tag{4}$$

Here

$$E' = \frac{E}{1-\nu^2}$$

$$s = \frac{2}{\pi}\tan^{-1}\left(\frac{t}{2a}\right)$$

where a is the crack depth, and t is the layer thickness.

The dependence of G on the normalized crack depth $a{\cdot}t^{-1}$ is plot in Fig. 4, and it shows that at $a \approx 0.28t$, the G function reaches its maximum value as

$$G_{\max} \approx \frac{0.42\sigma_s^2 t}{E'} \tag{5}$$

If the critical strain energy release rate of the sealing layer material is Γ, then no preexisting crack can extend into the layer when

$$G_{\max} < \Gamma \tag{6}$$

Combining Eqs. (5) and (6), one can find that the crack extension is possible only when

$$\frac{\Gamma E'}{t\sigma_s^2} \le 0.42 \tag{7}$$

The $\Gamma E'/(t\sigma_s^2)$ is normally defined as the normalized critical strain energy release rate (NCSERR). From Eqs. (2) and (7), it can be seen that $\Gamma E'/(t\sigma_s^2)$ is a function of the material properties and dimensions (e.g. the critical strain energy release rate, the elastic modulus, the coefficient of thermal expansion, and the layer thickness). The effects of these factors on the cracking behavior of the seals will be discussed later.

For a given system, as the stress increases to the level determined by Eq. (7) during cooling, a single flaw will be activated to extend into the layer only when its size is around $a = 0.28t$. If the preexisting flaw is much smaller, larger stresses need to develop before the crack spontaneously extends to a greater depth. Because G diminishes for large depths, the crack will stabilize at a larger depth [14] without further increase of the stress. Once a crack starts to extend in a catastrophic manner, the crack can extend to greater depths (greater values of a) when the residual thermal stress increases due to the further decrease of the temperature.

Consequently, for a given sealing system cooled to a prescribed temperature, there exists a critical seal thickness, t_c, below which cracks cannot extend, i.e. when

$$t \le t_c = \frac{\Gamma E'}{0.42\sigma_s^2} \tag{8}$$

3. Simulation results and discussion

As illustrated in Fig. 1, the typical multiple sealing sections in planar SOFCs include: metal frame/seal/metal foil/seal/metal frame (denoted as SS 1), and metal foil/seal/PEN (denoted as SS 2). The normalized critical strain energy release rate is different for the two types of sealing structures and will be illustrated separately.

The stresses in the glass or glass–ceramic sealing materials can be released to a very low level through plastic deformation at temperatures above the glass transition temperature (T_g). In the following simulation, the stresses in the sealing materials are therefore assumed to be zero at 800 °C as the glass transition temperatures of most sealing glasses are lower than 800 °C. Table 1 lists the typical values of the thermomechanical properties and dimensions of SOFC materials. The influence of these parameters on NCSERR will be systematically investigated, in such a condition that when one parameter is varied, the other parameters are fixed as 200 GPa for the interconnect elastic modulus, 70 GPa for the seal elastic modulus, $12.5 \times 10^{-6}\,K^{-1}$ for the interconnect CTE,

Table 1
Thermomechanical properties and dimensions of some typical SOFC materials.

Materials	Elastic modulus (GPa)	Poisson's ratio	CTE ($\times 10^6\,K^{-1}$)	Fracture energy ($J\,m^{-2}$)	Thickness (mm)
Cathode (LSM)	35 [16]	0.25 [16]	11.7 [17]	–	0.02
Electrolyte (8YSZ)	212 [18]	0.32 [19]	10.8[17]	–	0.01
Anode (Ni–8YSZ)	57 [18]	0.28 [19]	12.5 [20]	–	1.0
Frame/interconnect	150–250	~0.3	11–14	–	2.0
Metal foil	150–250	~0.3	11–14	–	0.05–0.5
Seals	60–100	~0.3	10–13	~5	0.1–0.5

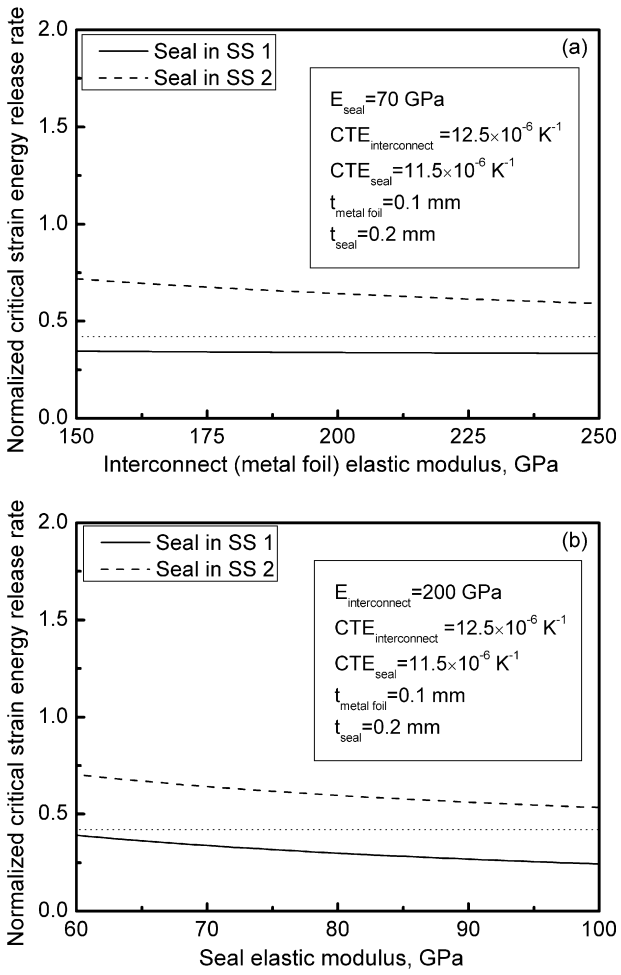

Fig. 5. The influence of the elastic modulus on the NCSERR: (a) the interconnect (metal foil) elastic modulus and (b) the seal elastic modulus.

$11.5 \times 10^{-6}\,K^{-1}$ for the seal CTE, 0.1 mm for the metal foil thickness and 0.2 mm for the seal thickness, respectively.

The influence of the elastic modulus on the NCSERR is shown in Fig. 5. It shows that the NCSERR of the seal in SS 1 is always less than the critical value of 0.42 while the NCSERR of the seal in SS 2 lies above the critical line, indicating that the sealing structure has pronounced influence on the NCSERR of the seal. It is clear that in the calculation condition, cracking of the seal in SS 1 is possible, indicating that the selected values are not suitable for the application of a real SOFC stack. How to optimize the parameters will be discussed later. Note that although an increase in the elastic modulus of the seal or the interconnect will lead to the decrease in the NCSERR of the seal, the variation range is quite limited. Therefore, the influence of the elastic modulus on the seal layer's resistance to cracking is very weak.

Fig. 6 shows the influence of the CTE of the seal and the interconnect (metal foil) on the NCSERR. It is seen that the NCSERR decreases with increasing CTE mismatch (absolute value of $\Delta\alpha$), especially in the small $\Delta\alpha$ (absolute value) region the NCSERR decreases rapidly. The figure also reveals that SS 2 can tolerate larger CTE mismatch than SS 1, as the critical $\Delta\alpha$ for cracking is around $0.9 \times 10^{-6}\,K^{-1}$ for SS 1, while for SS 2 the critical $\Delta\alpha$ is greater than $1.2 \times 10^{-6}\,K^{-1}$.

Fig. 7(a) shows the influence of the foil thickness on the NCSERR for the two types of seals. In the case of SS 2, the NCSERR decreases sharply with increase of the thickness up to 0.2 mm, after which the dependence of the NCSERR on the foil thickness is not so obvious. In the case of SS 1, the NCSERR shows nearly no variation with increasing foil thickness and the NCSERR is always less than 0.42, indicating that crack extension will be possible.

In a multilayer system, it is often the case that one component in the structure is far stiffer mechanically than the rest. In such cases the other components will be forced (as long as they are adherent) to be compatible with the displacements of the stiffest component, which remains almost stress free because of its greater stiffness, and hence the residual thermal stresses in them are mainly determined by the stiffest component when the system is cooled to a certain temperature. The stiffness is mainly controlled by the layer thickness and the elastic modulus of the layer material. In the case of SS 1, the interconnect layer is much thicker than the metal foil layer and it is the stiffest component, so the effect of the metal foil thickness on the residual thermal stresses in the seal is marginable, resulting in the insensitive of NCSERR to metal foil thickness. In the case of SS 2, the anode (1.0 mm) is the thickest layer and the metal foil (0.05–0.5 mm) is the second thickest layer without consideration of the seal layer, but the elastic modulus of the metal foil (200 GPa) is much higher than that of the anode (57 GPa), so both the anode and the metal foil are the stiff layers for SS 2. The residual thermal stresses in the seal layer are mainly determined by both the anode

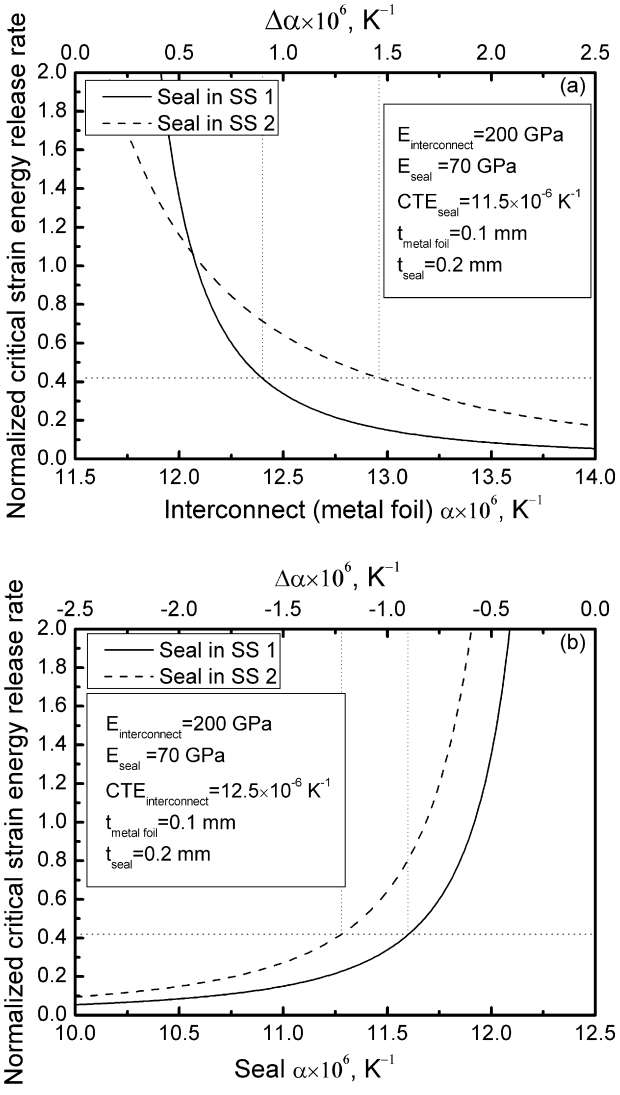

Fig. 6. The influence of the CTE on the NCSERR: (a) the interconnect (metal foil) CTE and (b) the seal CTE. Note that crack extension will not be possible when the normalized critical strain energy rate is greater than 0.42.

layer and the metal foil layer, resulting in the sensitive of NCSERR to metal foil thickness.

The influence of the seal thickness on the NCSERR is shown in Fig. 7(b). It is seen that for both SS 1 and SS 2, the NCSERR decreases significantly with increasing seal thickness, indicating that the seal thickness has crucial influence on its resistance to cracking.

From above analyses, it becomes clear that the influence of the CTE mismatch and the seal thickness on the NCSERR is significant, while other parameters like the elastic modulus have relatively weak correlation with the NCSERR. The CTE mismatch is closely correlated to the seal thickness as revealed by Eq. (8), by which for a predetermined $\Delta\alpha$, a critical seal thickness, t_c, below which the crack extension cannot occur, can be calculated. If the $\Delta\alpha$ is plotted against the t_c, cracking diagrams can then be obtained, as shown in Fig. 8. The lines in Fig. 8 represent the boundaries between the 'cracking' and the 'no cracking' area. Fig. 8(a) shows that the 'no cracking' area increases with the decreases of the CTE mismatch, which means that larger CTE mismatch would require a thinner seal to avoid cracking, e.g. when the CTE mismatch is greater than $1.2 \times 10^{-6}\,K^{-1}$, seals less than 0.1 mm should be employed to avoid cracking as illustrated in Fig. 8. On the other hand, when the CTE mismatch is less than $0.6 \times 10^{-6}\,K^{-1}$, the t_c increases rapidly with decreasing CTE mismatch and the dependence of the t_c on the $\Delta\alpha$ becomes not so critical. For example, the CTE mismatch of

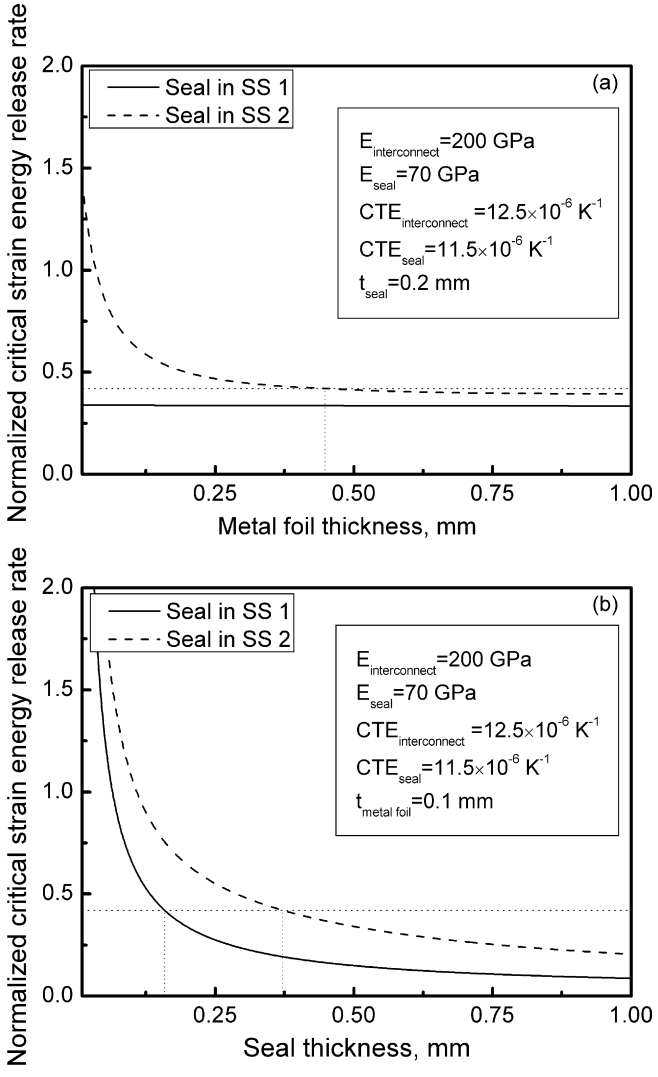

Fig. 7. The influence of the thickness on the NCSERR: (a) the metal foil thickness and (b) the seal thickness.

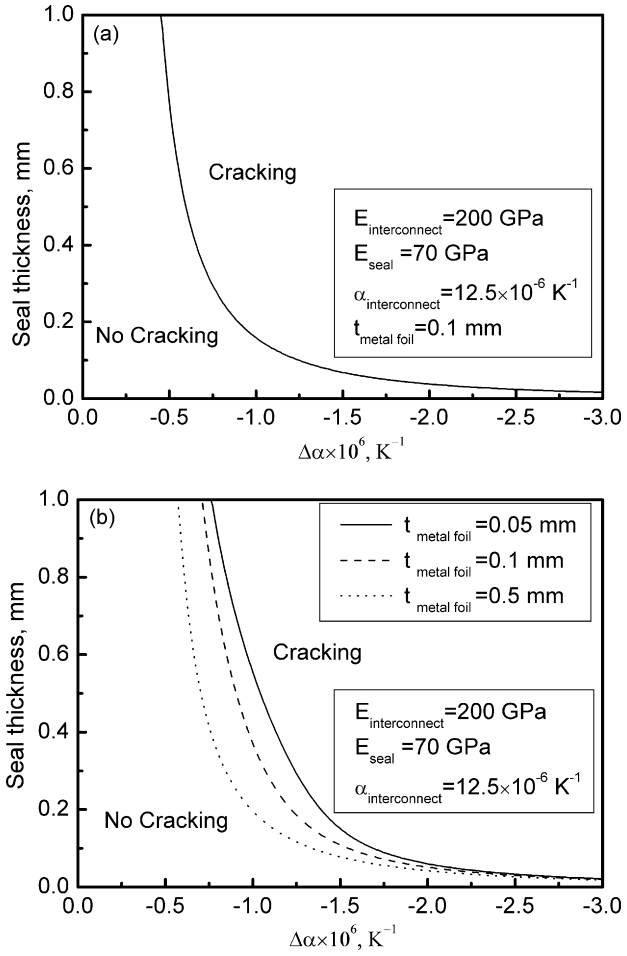

Fig. 8. Cracking diagrams of (a) SS 1 and (b) SS 2.

$0.5 \times 10^{-6}\,K^{-1}$ would allow a maximum seal thickness of 0.8 mm, which already exceeds the seal thickness of 0.1–0.5 mm as commonly reported in literature [7,9,21–24]. The cracking diagram for SS 2 is quite similar to that of SS 1, as shown in Fig. 8(b). However, since the thickness of the metal foil also has significant influence on the crack extension behavior, the 'no cracking/cracking' boundary is also dependent on the metal foil thickness. As shown in Fig. 8(b), the 'no cracking' area decreases with increasing thickness of the metal foil. From the comparison of Fig. 8(a) and (b), it can be seen that with the same CTE mismatch, the critical seal thickness for SS 1 is always thinner than that for SS 2. This is due to that the metal interconnect in SS 1 is much stiffer than the anode or the metal foil in SS 2.

In real applications, the choice for the SOFC interconnect materials is quite limited, so the match of the CTE is mainly depended on adjusting the CTE of the seals. Therefore, the seal CTE and the seal thickness are the two easily adjustable parameters for improving the seal reliability, and the cracking diagrams can be used as a useful tool for selecting the seal thickness after the seal and the other materials are determined in the design of a SOFC stack.

4. Validation

Experiments are designed to validate the influence of the seal thickness and the CTE mismatch on the crack extension behavior. Since it is difficult to instantaneously observe the crack initiation and extension, an alternative method, based on monitoring the leakage rate of a sealed gas chamber to detect the crack extension behavior, has been developed. For a sealed gas chamber, a

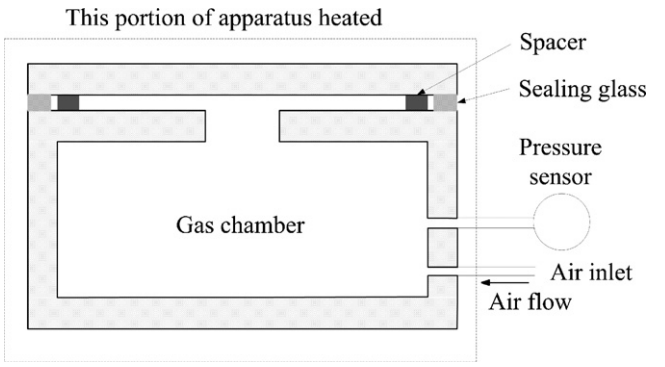

Fig. 9. Schematic of the leakage testing apparatus.

sudden increase of the leakage rate will indicate the open of the gas channels, which will be a clear indication of the crack extension. Consequently, by continuous monitoring the leakage rate of a sealed chamber, the onset of the crack extension can be easily determined.

Fig. 9 shows schematically the setup of the leakage testing. The gas chamber with the dimension of 70 mm × 70 mm × 50 mm was made of the interconnect alloy. The seal thickness was controlled by placing ceramic spacers of predetermined thickness between the two sealed surfaces, as illustrated in Fig. 9. A newly developed glass with the composition of 25 mol% SiO_2, 22 mol% B_2O_3, 30 mol% BaO, and 23 mol% other additives, was employed as the sealing material. The glass has a transition temperature of 582 °C and a CTE of $11.45 \times 10^{-6}\,K^{-1}$ (RT-582 °C), as measured by dilatometry (L75/1550, Linseis Messgeraete GmbH, Germany). Consequently, the minimum stress free temperature is set to 582 °C in the present study. The elastic modulus, the Poisson's ratio and the critical strain energy release rate of the glass are taken as 70 GPa, 0.3 and 5 J m^{-2}, respectively [25,26]. The CTE mismatch is adjusted experimentally by changing the alloy material, i.e. SS410 and SS430 with the CTEs of 12.03×10^{-6} and $12.24 \times 10^{-6}\,K^{-1}$ (RT-582 °C) respectively, are employed in the validation tests. The alloy, SS410 (Elastic modulus: 165 GPa; Poisson's ratio: 0.27), contains 11.5–13.5 wt.% Cr, <1 wt.% Si, <1 wt.% Mn, 0.03 wt.% C and the balance Fe, respectively. The alloy, SS430 (Elastic modulus: 170 GPa; Poisson's ratio: 0.27), contains 16–18 wt.% Cr, <1 wt.% Si, <1 wt.% Mn, 0.03 wt.% C and the balance Fe, respectively. Note that, the chromium content in SS410 is lower than that typically present in SOFC interconnect alloys.

After the parameters are fixed, the cracking diagram of this system is recalculated and shown in Fig. 10. By adjusting the CTE mismatch and the seal thickness, six samples including: two samples within the 'cracking' area, two samples along the 'cracking/no cracking' boundary, and the other two within the 'no cracking' area, as illustrated in Fig. 10, were designed to validate the cracking diagram. The materials, dimensions and CTE mismatches of the six samples are listed in Table 2.

Table 2
Materials, dimensions and CTE mismatches of the samples and the comparison between the measured and simulated results.

	Sample ID					
	1	2	3	4	5	6
Interconnect material	SS430	SS430	SS430	SS410	SS410	SS410
Seal thickness (mm)	0.3	0.5	1.0	0.5	1.0	3.0
$\Delta\alpha$ ($\times 10^6\,K^{-1}$)	−0.79	−0.79	−0.79	−0.58	−0.58	−0.58
Cracking or not						
Simulated	No	Boundary	Yes	No	Boundary	Yes
Measured	No	No	Yes	No	No	Yes

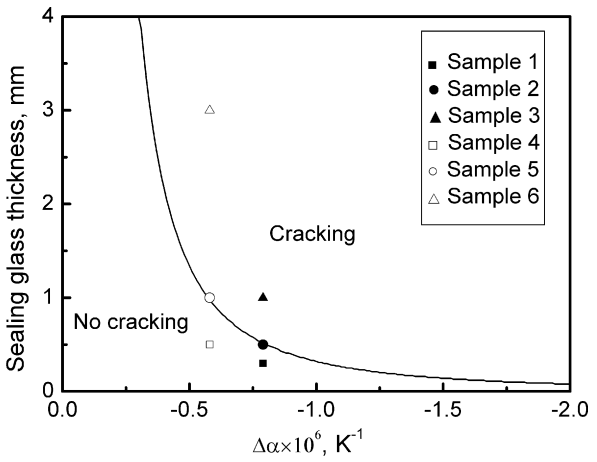

Fig. 10. Cracking diagram of the alloy–sealing glass–alloy system.

The gas chamber was sealed by the sealing glass in an electric furnace. The bonding was carried out by heating with a rate of 10 °C min^{-1} to 700 °C for 4 h in air. After the glass softened and bonded to the alloys during the heat treatment, the joined specimen was cooled to room temperature at a cooling rate of 0.5 °C min^{-1}. During cooling, the testing apparatus were held for 2 h at several temperatures to measure the leakage rates. The gas chamber was first pressurized to 10.0 kPa gauge pressure with air, the pipeline between the air source and the chamber was then closed, and the resulting pressure decay in the chamber was recorded with respect to time from 10.0 to 0.5 kPa. From the pressure decay data, leakage rate (LR, in standard cubic centimeters per minute per seal length at STP, sccm cm^{-1}), can be subsequently established as

$$\mathrm{LR} = \frac{22,414\,\mathrm{d}n}{L\,\mathrm{d}t} = \frac{22,414V\,\mathrm{d}p}{LRT\,\mathrm{d}t} \tag{9}$$

where n is the moles of the gas, T the temperature, V the chamber volume, R the gas constant, t the time, p the pressure, and L is the outer leak length (28.0 cm) of the gas chamber.

The leakage rates of the samples at a differential pressure of 1.4 kPa across the seal are shown in Fig. 11. It shows that for samples 3 and 6, the leakage rates increase abruptly at the temperatures of 300 and 100 °C, respectively, indicating that the gas channels in the seals extended in a catastrophic manner, i.e. the crack extension occurred when the samples were cooled to below these temperatures. A line crack could be observed throughout the central line of the free surfaces of the seal in each of the two samples when they were cooled to room temperature. Meanwhile, the other samples kept the low leakage rates during cooling. The leakage rates of the

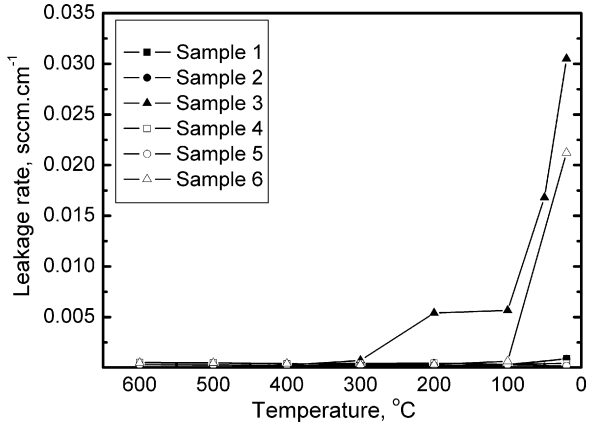

Fig. 11. Leakage rates at a differential pressure of 1.4 kPa across the seal.

samples without cracking were always below 1×10^{-3} sccm cm^{-1} (including the background leakage rate), fluctuating in the range of 1×10^{-4} to 1×10^{-3} sccm cm^{-1} due to the fluctuation of the room temperature or the temperature gradient in the samples.

A comparison between the measured and simulated results is listed in Table 2. Note that the simulated results are based on the assumption of the existence of the flaws with sizes around 0.28t, but in the sealing glass, the size of the flaws is usually smaller than 0.28t, so the cracks in the sealing glass with a thickness at the 'cracking/no cracking' boundary may not extend during cooling, which is testified by samples 2 and 5. From this table, it is clear that the predictions of cracking of the seals are well consistent with the experiments. Therefore, the model is valid for the crack extension behavior of the seals in SOFC, where the plane of the seal layer is subjected to biaxial compressive stresses. Both the simulated and experimental results imply that the resistance of the seal to cracking on cooling is significantly affected by the seal thickness and the CTE mismatch, and a seal with less thickness and CTE mismatch between itself and the adjacent layers is more reliable.

5. Conclusions

In the present paper, a model based on the classical beam bending theory and the fracture theory of ceramic materials has been developed for predicting cracking of the glass-based seal, which is under biaxial compressive stresses, for SOFC. Since the CTE of the common seal used in SOFC stacks is lower than that of the interconnect or the anode, and hence the bodies of the seal are under biaxial compressive stresses, the model can be used to analyze the cracking behavior of the seal in SOFC. The analysis indicates that the resistance of the seal to cracking on cooling is significantly affected by the seal thickness and the CTE mismatch. For a given CTE mismatch between the seal and the sealed material (e.g. the interconnect metal), there exists a critical seal thickness, above which, the strain energy release rate of the seal will exceed its critical value and lead to cracking.

A cracking diagram has been established to reveal the effects of the seal thickness and the CTE mismatch on the crack extension behavior. It shows that the 'no cracking' area increases with decreasing seal thickness, and larger CTE mismatch would require a thinner seal to avoid cracking. The model and the cracking diagram were experimentally validated through monitoring the leakage rate of a glass-sealed chamber. The crack extension deduced from the measured leakage rate showed good agreement with those predicted by the model. Both the simulated and experimental results indicate that the reliability of the seal could be improved by reducing seal thickness and CTE mismatch. In addition, the cracking diagram can serve as a guideline in selection of the sealing material and design of the sealing structure.

Acknowledgements

The helpful discussions with Professor Zhigang Suo, from Harvard University, are appreciated by the authors. The financial support of the National Natural Science Foundation of China (Grant No. 50730002) is gratefully acknowledged.

References

[1] S.P. Simner, J.W. Stevenson, J. Power Sources 102 (2001) 310–316.
[2] J. Malzbender, R.W. Steinbrech, J. Power Sources 173 (2007) 60–67.
[3] K.S. Weil, C.A. Coyle, J.S. Hardy, J.Y. Kim, G.-G. Xia, Fuel Cells Bull. 2004 (2004) 11–16.
[4] R.N. Singh, J. Mater. Eng. Perform. 15 (2006) 422–426.
[5] R.N. Singh, Int. J. Ceram Appl. Technol. 4 (2007) 134–144.
[6] Y.S. Chou, J.W. Stevenson, R.N. Gow, J. Power Sources 170 (2007) 395–400.
[7] K.A. Nielsen, M. Solvang, S.B.L. Nielsen, A.R. Dinesen, D. Beeaff, P.H. Larsen, J. Eur. Ceram. Soc. 27 (2007) 1817–1822.
[8] M.J. Pascual, A. Guillet, A. Duran, J. Power Sources 169 (2007) 40–46.
[9] F. Smeacetto, M. Salvo, M. Ferraris, V. Casalegno, P. Asinari, J. Eur. Ceram. Soc. 28 (2008) 611–616.
[10] F. Smeacetto, M. Salvo, M. Ferraris, J. Cho, A.R. Boccaccini, J. Eur. Ceram. Soc. 28 (2008) 61–68.
[11] S. Ghosh, P. Kundu, A. Das Sharma, R.N. Basu, H.S. Maiti, J. Eur. Ceram. Soc. 28 (2008) 69–76.
[12] A. Muller, W. Becker, D. Stolten, J. Hohe, Eng. Fract. Mech. 73 (2006) 994–1008.
[13] T. Zhang, Q. Zhu, W.L. Huang, Z. Xie, X. Xin, J. Power Sources 182 (2008) 540–545.
[14] S. Ho, C. Hillman, F.F. Lange, Z. Suo, J. Am. Ceram. Soc. 78 (1995) 2353–2359.
[15] H. Tada, P.C. Paris, G.R. Irwin, The Stress Analysis of Cracks Handbook, third ed., The American Society of Mechanical Engineers, New York, 2000, p. 211.
[16] N.M. Sammes, Y. Du, Electrochem. Proc. 97 (18) (2000) 671–679.
[17] A. Nakajo, C. Stiller, G. Harkegard, O. Bolland, J. Power Sources 158 (2006) 287–294.
[18] M. Radovic, E. Lara-Curzio, Acta Mater. 52 (2004) 5747–5756.
[19] A. Atkinson, A. Selcuk, Solid State Ionics 134 (2000) 59–66.
[20] F. Tietz, Ionics 5 (1999) 129–139.
[21] K.S. Weil, B.J. Koeppel, Int. J. Hydrog. Energy 33 (2008) 3976–3990.
[22] S. Taniguchi, M. Kadowaki, T. Yasuo, Y. Akiyama, Y. Miyake, K. Nishio, J. Power Sources 90 (2000) 163–169.
[23] Y.S. Chou, J.W. Stevenson, J. Hardy, P. Singh, J. Power Sources 157 (2006) 260–270.
[24] S.M. Gross, T. Koppitz, J. Remmel, J.-B. Bouche, U. Reisgen, Fuel Cells Bull. 2006 (2006) 12–15.
[25] S. Ho, Z. Suo, J. Appl. Mech.-Trans. ASME 60 (1993) 890–894.
[26] B.N. Nguyen, B.J. Koeppel, S. Ahzi, M.A. Khaleel, P. Singh, J. Am. Ceram. Soc. 89 (2006) 1358–1368.